Bidirectional interactions between neuronal and hemodynamic responses to transcranial direct current stimulation (tDCS): challenges for brain-state dependent tDCS

Anirban Dutta

HAL Id: hal-01203367

https://inria.hal.science/hal-01203367

Submitted on 16 Apr 2019

Bidirectional interactions between neuronal and hemodynamic responses to transcranial direct current stimulation (tDCS): challenges for brain-state dependent tDCS

Anirban Dutta[1,2*]

[1]INRIA (Sophia Antipolis) – CNRS : UMR5506 – Université Montpellier, Montpellier, France
[2]Laboratoire d'Informatique de Robotique et de Microélectronique de Montpellier (LIRMM), CNRS : UMR5506 – Université Montpellier, Montpellier, France

*Correspondence: Anirban Dutta, INRIA – CNRS : UMR5506 – Université Montpellier, Montpellier, France
Email: adutta@ieee.org

Abstract

Transcranial direct current stimulation (tDCS) has been shown to modulate cortical neural activity. During neural activity, the electric currents from excitable membranes of brain tissue superimpose in the extracellular medium and generate a potential at scalp, which is referred as the electroencephalogram (EEG). Respective neural activity (energy demand) has been shown to be closely related, spatially and temporally, to cerebral blood flow (CBF) that supplies glucose (energy supply) via neurovascular coupling. The hemodynamic response can be captured by near-infrared spectroscopy (NIRS), which enables continuous monitoring of cerebral oxygenation and blood volume. This neurovascular coupling phenomenon led to the concept of neurovascular unit (NVU) that consists of the endothelium, glia, neurons, pericytes, and the basal lamina. Here, recent works suggest NVU as an integrated system working in concert using feedback mechanisms to enable proper brain homeostasis and function where the challenge remains in capturing these mostly nonlinear spatiotemporal interactions within NVU for brain-state dependent tDCS. In principal accordance, we propose EEG-NIRS-based whole-head monitoring of tDCS-induced neuronal and hemodynamic alterations during tDCS.

Challenges in clinical translation of transcranial brain stimulation - an introduction

Transcranial direct current stimulation (tDCS) - an electrically based intervention directed at the central nervous system level - is a promising tool to alter cortical excitability and facilitate neuroplasticity (Nitsche and Paulus, 2011). However, inter-subject variability and intra-subject reliability currently limits clinical translation (Horvath et al., 2014). Indeed, a recent meta-analysis showed that the treatment effects of transcranial brain stimulation in patients with stroke are rather inconsistent across studies and the evidence for therapeutic efficacy is still uncertain (Raffin and Siebner, 2014). Here, it may be possible to reduce inter-subject variability and improve intra-subject reliability using simultaneous neuroimaging that can objectively quantify the individual brain-state before and during tDCS. Non-invasive neuroimaging techniques that have previously been combined with tDCS include electrophysiological, e.g., EEG (Schestatsky et al., 2013) and haemodynamic, e.g., functional magnetic resonance imaging (fMRI) (Meinzer et al., 2014) and NIRS (McKendrick et al., 2015) approaches. Here, NIRS presents several advantages relative to fMRI, such as measurement of concentration changes in both oxygenated (HbO2) and deoxygenated (HHb) hemoglobin, finer temporal resolution, ease of administration and relative insensitivity to movement

42 artefacts. Although fMRI has become the benchmark for in-vivo imaging of the human brain, in
43 practice, NIRS and EEG are more convenient and less expensive technology than fMRI for
44 simultaneous neuroimaging for brain-state dependent tDCS. However, the challenge remains in
45 modeling whole-head spatiotemporal coupling of neuronal and hemodynamic alterations induced by
46 tDCS where such brain-state dependent tDCS needs not only to consider the brain as a dynamical
47 system but also need to consider that its parameters will be inter-individually heterogeneous,
48 dependent on brain injury (and maladaptive plasticity, e.g., reactive gliosis (Buffo et al., 2008)), task
49 characteristics (e.g., attention issues) and other factors (Raffin and Siebner, 2014).

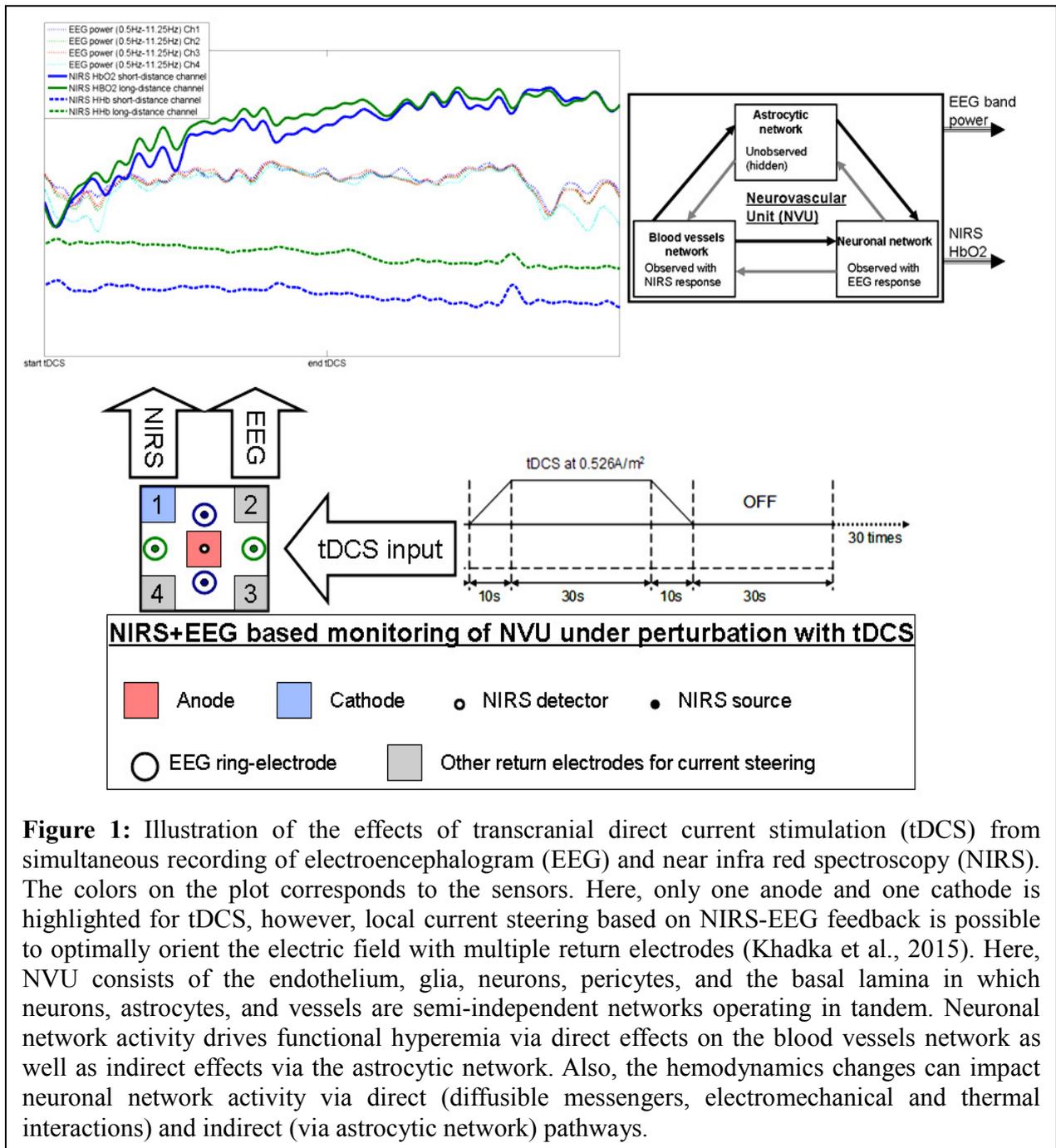50 **Biophysical models for capturing hemodynamic alterations induced by tDCS**
51 Neural activity has been shown to be closely related, spatially and temporally, to cerebral blood flow
52 (CBF) that supplies glucose via neurovascular coupling (Girouard and Iadecola, 2006). The
53 hemodynamic response to neural activity can be captured by near-infrared spectroscopy (NIRS),
54 which enables continuous monitoring of cerebral oxygenation and blood volume (Siesler et al.,
55 2008). The regulation of CBF and its spatiotemporal dynamics may be probed with short-duration
56 anodal tDCS which challenges the system with a vasoactive stimulus in order to observe the system
57 response. Based on prior works (Nitsche and Paulus, 2000)(Dutta et al., 2015), such short-duration
58 (<1min) anodal tDCS is postulated to cause no aftereffects and may be used to probe neurovascular
59 coupling (and NVU) (Jindal et al., 2015b). Here, CBF is increased in brain regions with enhanced
60 neural activity via metabolic coupling mechanisms (Attwell et al., 2010) while cerebral
61 autoregulation mechanisms ensure that the blood flow is maintained during changes of perfusion
62 pressure (Lucas et al., 2010). During such a short-duration anodal tDCS experiment, cerebrovascular
63 reactivity (CVR) can be measured as the change in CBF per unit change in relation to anodal tDCS
64 intensity. Moreover, the rate of change of hemodynamic responses to same tDCS intensity may
65 explain inter-individual differences in tDCS after-effects (Han et al., 2014). Also, phenomological
66 model for metabolic coupling mechanisms (Attwell et al., 2010) can be used to capture CVR that
67 represents the capacity of blood vessels to dilate during anodal tDCS due to neuronal activity-related
68 increased demands of oxygen (Dutta et al., 2013). Here, CVR reflects the capacity of blood vessels to
69 dilate, and is an important marker for brain vascular reserve (Markus and Cullinane, 2001). Indeed
70 pressure–perfusion–cognition relationships may be monitored with the brain vascular reserve
71 (Novak, 2012) where the CVR distributes CBF toward the brain areas in need of increased perfusion
72 due to enhanced neural activity.

73
74 Prior work has shown a significant correlation between tDCS current strength and increase in
75 regional CBF in the on-period relative to the pre-stimulation baseline (Zheng et al., 2011). We
76 investigated regional CVR during anodal tDCS by adapting an arteriolar compliance model of the
77 cerebral blood flow response to a neural stimulus (Behzadi and Liu, 2005). Regional CVR was
78 defined as the coupling between changes in CBF and cerebral metabolic rate of oxygen (CMRO2)
79 during anodal tDCS-induced local brain activation (Leontiev and Buxton, 2007). The complex path
80 from the tDCS-induced change of the synaptic transmembrane current, $u(t)$ (only excitatory effects
81 considered) (Molaee-Ardekani et al., 2013) to a change in the concentration of multiple vasoactive
82 agents (such as NO, potassium ions, adenosine), represented by a single vascular flow-inducing
83 vasoactive signal, s, was captured by a first-order Friston's model (Friston et al., 2000). Chander and
84 Chakravarthy (Chander and Chakravarthy, 2012) presented a computational model that studied the
85 effect of metabolic feedback on neuronal activity to bridge the gap between measured hemodynamic
86 response and ongoing neural activity. Here, the NVU (see Figure 1) consists of the endothelium, glia,
87 neurons, pericytes, and the basal lamina that has been proposed to maintain the homeostasis of the
88 brain microenvironment (Iadecola, 2004). In this connection, the role of lactate as a signaling

89 molecule was described recently (Yang et al., 2014), which supports a (delayed) "reverse" influence
90 in the NVU from the vessel back to neuron via lactate (Chander and Chakravarthy, 2012). Recently, a
91 detailed biophysical model of the brain's metabolic interactions was presented by Jolivet et al.
92 (Jolivet et al., 2015). This not only supported the astrocyte-neuron lactate shuttle (ANLS) hypothesis
93 that the lactate produced in astrocytes (a type of glial cell) can also fuel neuronal activity but it also
94 provided a quantitative mathematical description of the metabolic activation in neurons and glial
95 cells, as well as of the macroscopic measurements obtained during brain imaging. Indeed, this model
96 captured the pattern of neurovascular responses observed in rodents in response to sustained sensory
97 stimulation where CBF only starts to increase above its baseline ~0.5–1 sec after the onset of
98 stimulation (Jolivet et al., 2015). We also found such onset effects (called "initial dip") of anodal
99 tDCS in stroke patients (Dutta et al., 2015). Moreover, Jolivet et al. (Jolivet et al., 2015) highlighted
100 the neuron-astrocyte cross-talk during oscillations linked to blood oxygenation levels (DiNuzzo et al.,
101 2011) where such oscillations also occurred after anodal tDCS-based perturbation of the neuroglial
102 networks in our EEG-NIRS stroke study (Dutta et al., 2015). We therefore postulate that short-
103 duration anodal tDCS can be used to perturb neuroglial networks in health and disease to probe the
104 spatiotemporal dynamics of the NVU based on simultaneous EEG-NIRS neuroimaging (Dutta, 2014)
105 (Dutta et al., 2015) and biophysical model (Jolivet et al., 2015) based analysis.

Hemo-neural hypothesis for brain-state dependent tDCS

Figure 1: Illustration of the effects of transcranial direct current stimulation (tDCS) from simultaneous recording of electroencephalogram (EEG) and near infra red spectroscopy (NIRS). The colors on the plot corresponds to the sensors. Here, only one anode and one cathode is highlighted for tDCS, however, local current steering based on NIRS-EEG feedback is possible to optimally orient the electric field with multiple return electrodes (Khadka et al., 2015). Here, NVU consists of the endothelium, glia, neurons, pericytes, and the basal lamina in which neurons, astrocytes, and vessels are semi-independent networks operating in tandem. Neuronal network activity drives functional hyperemia via direct effects on the blood vessels network as well as indirect effects via the astrocytic network. Also, the hemodynamics changes can impact neuronal network activity via direct (diffusible messengers, electromechanical and thermal interactions) and indirect (via astrocytic network) pathways.

Neural mass or field models for capturing neuronal alterations induced by tDCS

During neural activity, the electric currents from excitable membranes of brain tissue superimpose at a given location in the extracellular medium and generate a potential, which is referred to as the EEG (Nunez and Srinivasan, 2006). Here, neural mass models (NMM) can provide insights into the neuromodulatory mechanisms underlying alterations of cortical activity induced via tDCS (Molaee-Ardekani et al., 2013). Specifically, the origin of tDCS-induced alterations in the EEG power spectrum was captured using a thalamocortical NMM (Dutta and Nitsche, 2013). The NMM for a single cortical source comprises of 4 neuronal subpopulations, excitatory pyramidal neurons (ePN), excitatory interneurons (eIN), slow inhibitory interneurons (siIN), and fast inhibitory interneurons

116 (fiIN) (Zavaglia et al., 2006). The NMM for the cortical source was coupled with another
117 representing the thalamus (Sotero et al., 2007), which comprises of 2 neuronal subpopulations - an
118 excitatory thalamocortical (eTCN) and an inhibitory reticular-thalamic (iRT). The basis of our
119 cortical NMM is the Friston model (Moran et al., 2007) that emulates the activity of a cortical area
120 using three neuronal subpopulations, ePN, eIN, and siIN. A population of ePN (output) cells receives
121 inputs from inhibitory and excitatory populations of interneurons via intrinsic connections (intrinsic
122 connections are confined to the cortical sheet). An extrinsic thalamo–cortico–thalamic loop consists
123 of eTCN and iRT in the thalamic NMM (Ursino et al., 2010). Our lumped thalamo–cortico–thalamic
124 network model can be used to simulate the subject-specific EEG power spectral density changes
125 during/following tDCS (Dutta and Nitsche, 2013) by modifying the model parameters (e.g., average
126 gain of synapses, their time constants) (Zavaglia et al., 2006). We found that anodal tDCS enhances
127 activity and excitability of the excitatory pyramidal neuron at a population level in a non-specific
128 manner and mu-rhythm desynchronization is generated (Dutta and Nitsche, 2013). The tDCS effects
129 on the population kinetics depend on the direction of cortical current flow determining the relative
130 influence of acute tDCS on the cellular targets responsible for modulation of synaptic efficacy, which
131 are primarily somata and axon terminals (Rahman et al., 2013). Basal and apical dendrites can be
132 concomitantly polarized in opposite directions, and Layer V pyramidal neurons exhibit the highest
133 measured somatic sensitivities to subthreshold fields (Rahman et al., 2013). Therefore, not all neural
134 tissue will be equally affected by a given stimulation protocol which may distinctly affect neuronal
135 populations/neuronal compartments. Indeed, a recent computational modeling study suggested that
136 tDCS may induce opposing effects on different types of interneurons (Molaee-Ardekani et al., 2013).
137 Here, the excitation versus inhibition effects (Krause et al., 2013) of tDCS on the population kinetics
138 can produce a whole spectrum of EEG signals within the oscillatory regime of a neural mass model
139 (David and Friston, 2003).

140 There are several prior works that have shown both "online" effects of tDCS on EEG with EEG
141 performed during tDCS as well as "offline" effects with EEG performed after tDCS. Here, it is
142 important to separate studies where tDCS is applied during a rest state (Ardolino et al., 2005) (Zaehle
143 et al., 2011) (Spitoni et al., 2013) or an active task state (Matsumoto et al., 2010) (Mangia et al.,
144 2014). We computationally found (Dutta and Nitsche, 2013) in concordance with the experimental
145 results of Matsumoto et al. (Matsumoto et al., 2010) that tDCS effects on mu-rhythm
146 desynchronization depend on the direction of cortical current flow determining the relative influence
147 of acute tDCS on the cellular targets. Matsumoto et al. (Matsumoto et al., 2010) found that tDCS
148 applied over the left primary motor area for 10min at 1mA with a 35cm^2 electrode influenced event-
149 related desynchronization (ERD) during right hand grasping where the mu ERD increased after
150 anodal tDCS and decreased after cathodal tDCS. Here, not only the "local" effects but the "distant"
151 effects of tDCS are also relevant where Polanía et al. (Polanía et al., 2012) reported that the
152 functional connectivity patterns significantly increased after anodal tDCS (i.e., "offline" effects) over
153 the primary motor cortex where tDCS modulated functional connectivity of cortico-striatal and
154 thalamo-cortical circuits. Notturno et al. (Notturno et al., 2014) showed spatial diffusion of anodal
155 tDCS (during a motor task) effects where an increment of low alpha band power over the course of
156 pre- and post-stimulation recording sessions was found during motor task that was localized in the
157 sensorimotor and parieto-occipital regions. Indeed, not only the "offline" effects, but changes in
158 functional connectivity patterns may start evolving during tDCS (i.e., "online" effects) as shown by
159 our modeling study (Dutta and Nitsche, 2013). tDCS/EEG co-registration studies have shown that
160 anodal tDCS mostly modulate spontaneous cortical activity in the alpha band where alpha-rhythm
161 states have a significant effect on perceptual learning (Sigala et al., 2014). In fact, more than 60% of
162 the observed inter-subject variability in perceptual learning can be ascribed to ongoing alpha activity
163 where Sigala et al. (Sigala et al., 2014) highlighted the need for multidisciplinary approaches

164 combining assessment of behavior and multi-scale neuronal activity, active modulation of ongoing
165 brain states and computational modeling to reveal the mathematical principles of the complex
166 neuronal interactions. We therefore postulate that concurrent EEG-NIRS-based neuroimaging of the
167 short-duration tDCS-induced modulation can be analyzed by combining a biophysical model (Jolivet
168 et al., 2015) of the NVU with the computational model (neural mass or field model) of multi-scale
169 neuronal activity of the whole brain (Sigala et al., 2014) to capture the spatiotemporal dynamics of
170 the interactions between the neuronal and hemodynamic responses in health and disease. Here, the
171 challenges remain in ensuring the observability of the NVU with intelligent placement of EEG-NIRS
172 sensors since presence of symmetry in the nonlinear network of NVU (see Figure 1) may decrease
173 observability (although networks containing only rotational symmetries remain observable) (Whalen
174 et al., 2015).

175 **Bidirectional interactions between neuronal and hemodynamic responses to tDCS - a discussion**

176 In our prior work (Dutta et al., 2015), we found an initial dip in the oxy-haemoglobin concentration
177 and concomitant increase in the mean power spectral density within lower (<12Hz) EEG frequency
178 band. It was postulated that the immediate need to fuel neuronal energy recovery was via the lactate
179 shuttle (Pellerin and Magistretti, 1994) where blood glucose supply has a longer delay (Gruetter et
180 al., 1996). A detailed biophysical model of the brain's metabolic interactions by Jolivet et al. (Jolivet
181 et al., 2015) also supported the ANLS hypothesis. Moreover, recent works showed that lactate can
182 modulate the activity of primary cortical neurons through a receptor-mediated pathway (Bozzo et al.,
183 2013) and vasomotion rhythms can influence neural firing patterns (Nikulin et al., 2014). Also,
184 lactate promotes plasticity gene expression by potentiating NMDA signaling in neurons, and the
185 action of lactate is mediated by the modulation of NMDA receptor activity (Yang et al., 2014). These
186 dynamic ANLS interactions leave us to question its role in tDCS facilitated neuroplasticity and
187 learning (Suzuki et al., 2011). Also, the spatiotemporal dynamics of the millisecond-to-second-range
188 direct (diffusible messengers, electromechanical and thermal interactions) and seconds-to-tens-of-
189 seconds-range indirect interaction in the NVU following tDCS, i.e. the hemo-neural hypothesis
190 (Moore and Cao, 2008), may at least partially explain the time course of the induction of homeostatic
191 plasticity generated by repeated tDCS of the human motor cortex (Fricke et al., 2011). Fricke and
192 coworkers (Fricke et al., 2011) hypothesized a role of L-type voltage-gated Ca2+ channels (L-
193 VGCC) in short-term homeostatic plasticity, since tDCS has been shown to induce a long-lasting
194 disturbance of Ca2+ homeostasis (Islam et al., 1995) and induce calcium-dependent plasticity
195 (Nitsche et al., 2003). Here, the glial network may have an important role (i.e., spatial buffering) in
196 regulating neural activity by distributing ions (Halnes et al., 2013) in seconds-to-tens-of-seconds-
197 range where an influence of long-lasting disturbance of Ca2+ homeostasis via tDCS on the myogenic
198 and the metabolic control of cerebral circulation cannot be excluded. In fact, astrocytes, a sub-type of
199 glia in the central nervous system, can integrate a large number of synapses and can respond to
200 neuronal activity via neurotransmitter-evoked activation of astrocytic receptors (Araque et al., 2001).
201 Indeed, neuronal activity can mobilize internal calcium in astrocytes and the calcium wave in
202 different spatial–temporal dimensions can result in a higher level of brain integration (Volterra et al.,
203 2014) where the evidence for tDCS-induced large scale changes in brain synchronization and
204 topological functional organization has been shown after acute stimulation (Polanía et al., 2011).
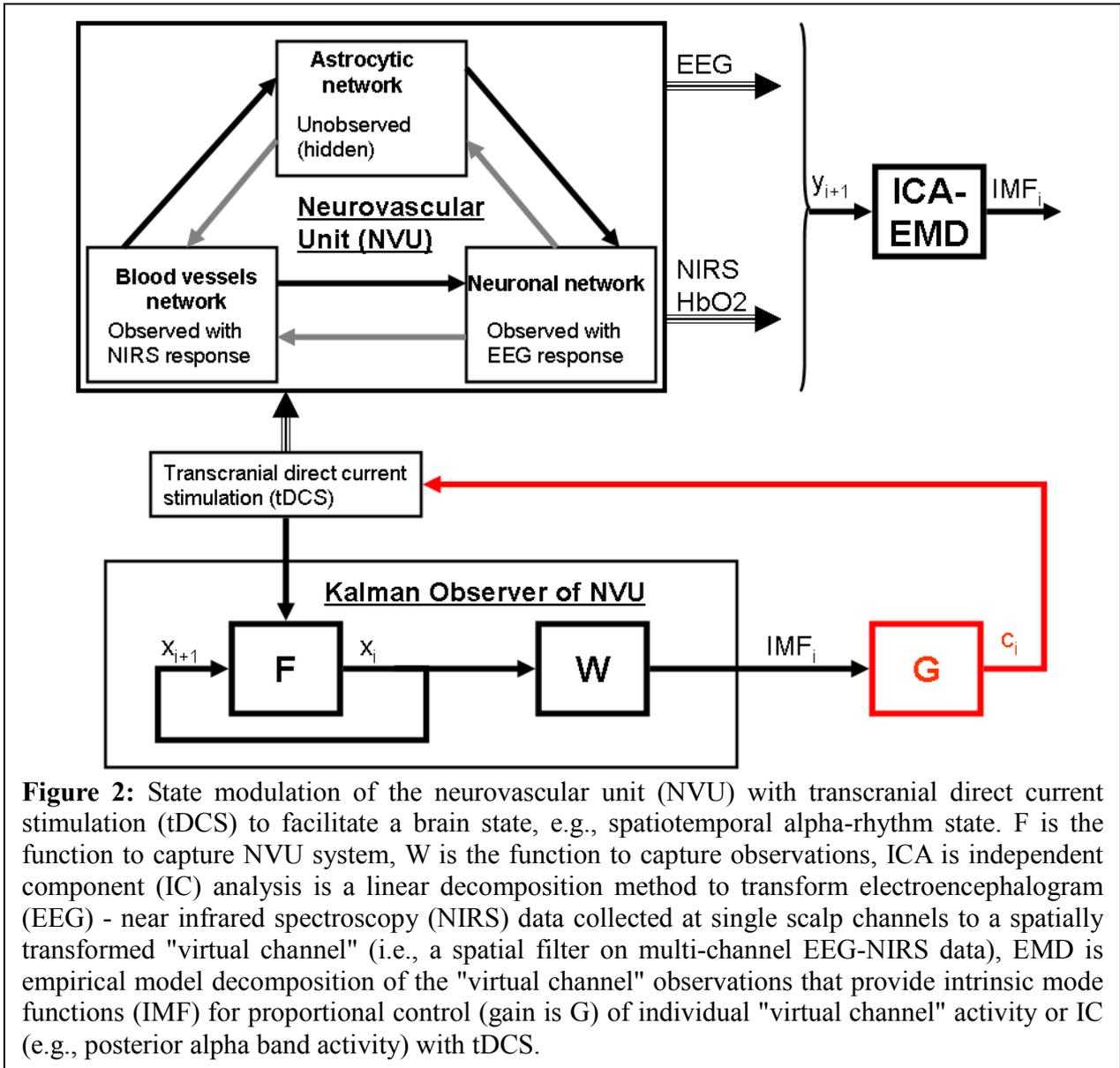205
206 Based on these prior works, we recently proposed EEG-NIRS-based monitoring of neurovascular
207 coupling functionality under perturbation with tDCS (Jindal et al., 2015b). Here, neuronal and
208 hemodynamic responses measured with EEG-NIRS neuroimaging can be represented abstractly as
209 the system response of the NVU to tDCS perturbation (see Figure 1) where presence of symmetry in

210 the nonlinear network of NVU (see Figure 1) may decrease observability (Whalen et al., 2015). Since
211 no real-world network has exact symmetries so with intelligent placement of EEG-NIRS sensors (e.g.
212 to avoid systemic interference (Sood et al., 2015)) along with system identification and parameter
213 estimation techniques, it may be possible to track the spatiotemporal change of the states of the NVU.
214 This observer model can then be used to drive multi-electrode tDCS (Dmochowski et al., 2011) for
215 active spatiotemporal modulation of the brain states (e.g., posterior alpha-rhythm). Here, we base our
216 discussions on the recent advances in Kalman filtering approaches to spatiotemporal nonlinear
217 systems (Schiff and Sauer, 2008) and an understanding from group representation theory in controller
218 or observer design by obtaining a modal decomposition into decoupled controllable and
219 uncontrollable (observable and unobservable) subspaces (Whalen et al., 2015). Specifically, Schiff
220 and Sauer (Schiff and Sauer, 2008) showed the feasibility of unscented Kalman filter (UKF) for
221 recursive estimation of system state for nonlinear systems, including unobserved variables and
222 parameter tracking, in a spatiotemporal model of cortex where such a nonlinear system is controllable
223 using an adaptive feedback electrical field. Here, discretization of the whole-brain detailed
224 biophysical model of NVU (Jolivet et al., 2015), for example with Galerkin methods that are used
225 quite robustly in fluid dynamics, will be necessary where each discrete element corresponds to a
226 volume of tissue imaged as well as stimulated with the EEG-NIRS/tDCS unit (see Figure 1). As an
227 alternative to a fundamental NVU model (Jolivet et al., 2015) for the volume of tissue imaged and
228 stimulated with EEG-NIRS/tDCS unit, we tried (Dutta et al., 2015) to find an empirical model where
229 we performed empirical mode decomposition (EMD) and the Hilbert spectrum (Huang et al., 1998)
230 to model the system dynamics and found a negative cross-correlation between one of the intrinsic
231 mode function (IMF) of the HbO2 time-series and log-transformed mean-power time-course of EEG
232 primarily within 0.5Hz-11.25Hz frequency band (i.e., one of the EEG IMFs). In principal accordance,
233 for whole-head monitoring, we propose independent component analysis (ICA) to transform multi-
234 channel EEG-NIRS/tDCS unit imaging data to a spatially transformed "virtual channel" (i.e., a
235 spatial filter) (Jung et al., 2001). Then, the "virtual channel" activity (e.g., posterior alpha band
236 activity) can be subjected to EMD (i.e., a temporal filter) to reduce the dimension of the observable
237 dynamics (i.e., further observer model reduction) before developing the Kalman filter observer
238 (Schiff and Sauer, 2008) using the IMFs. For EEG-NIRS-based monitoring of NVU under
239 perturbation with tDCS, as shown in the Figure 2, the NVU dynamics is captured by the function F
240 and the IMF observations by the function W. The UKF approach should match the nonlinear IMF
241 dynamics up to the second order statistics where the feasibility remains to be tested experimentally in
242 future studies. Furthermore, it may be possible to use the Kalman observer to calculate proportional
243 control (see Figure 2) of the brain-state (e.g., cortical excitability (Jindal et al., 2015a)) with tDCS.
244 Here, intelligent placement of EEG-NIRS sensors and tDCS effectors is necessary to ensure
245 observability and controllability (Whalen et al., 2015) where Whalen et al. (Whalen et al., 2015)
246 suggested in general that more direct incoming connections into an observed node lead to higher
247 observability and more direct outgoing connections from a controlled node lead to higher
248 controllability. Furthermore, controllability may be enhanced with multi-modal non-invasive brain
249 stimulation (NIBS), e.g. with direct electrical stimulation (Pulgar, 2015) and photobiostimulation
250 (Gonzalez-Lima and Barrett, 2014), which needs to be investigated.

251 Towards such brain-state dependent tDCS, the challenges include the nature of observability and
252 controllability in whole-brain complex NVU networks as well as the subtleties of the tDCS
253 interaction with the whole-brain NVU (e.g., based on heterogeneous geometrical characteristics
254 (Molaee-Ardekani et al., 2013)) that can also have multi-timescale cross-talk and resulting complex
255 non-linear dynamics (Jolivet et al., 2015) where the spatiotemporal observability and controllability
256 remains to be verified in future studies.

257

Figure 2: State modulation of the neurovascular unit (NVU) with transcranial direct current stimulation (tDCS) to facilitate a brain state, e.g., spatiotemporal alpha-rhythm state. F is the function to capture NVU system, W is the function to capture observations, ICA is independent component (IC) analysis is a linear decomposition method to transform electroencephalogram (EEG) - near infrared spectroscopy (NIRS) data collected at single scalp channels to a spatially transformed "virtual channel" (i.e., a spatial filter on multi-channel EEG-NIRS data), EMD is empirical model decomposition of the "virtual channel" observations that provide intrinsic mode functions (IMF) for proportional control (gain is G) of individual "virtual channel" activity or IC (e.g., posterior alpha band activity) with tDCS.

258

259 **Acknowledgments**

263 Das, Dr. Shubhajit Roy Chowdhury, and Dr. Dipanjan Roy), and the French collaborators (Dr.
264 Mitsuhiro Hayashibe, Dr. Stephane Perrey and Dr. Mark Muthalib) are gratefully acknowledged.

265 **References**

266 Araque, A., Carmignoto, G., and Haydon, P. G. (2001). Dynamic signaling between astrocytes and
267   neurons. *Annu. Rev. Physiol.* 63, 795–813. doi:10.1146/annurev.physiol.63.1.795.

268 Ardolino, G., Bossi, B., Barbieri, S., and Priori, A. (2005). Non-synaptic mechanisms underlie the
269   after-effects of cathodal transcutaneous direct current stimulation of the human brain. *J.
270   Physiol.* 568, 653–663. doi:10.1113/jphysiol.2005.088310.

271 Attwell, D., Buchan, A. M., Charpak, S., Lauritzen, M., Macvicar, B. A., and Newman, E. A. (2010).
272   Glial and neuronal control of brain blood flow. *Nature* 468, 232–243.
273   doi:10.1038/nature09613.

274 Behzadi, Y., and Liu, T. T. (2005). An arteriolar compliance model of the cerebral blood flow
275   response to neural stimulus. *NeuroImage* 25, 1100–1111.
276   doi:10.1016/j.neuroimage.2004.12.057.

277 Bozzo, L., Puyal, J., and Chatton, J.-Y. (2013). Lactate Modulates the Activity of Primary Cortical
278   Neurons through a Receptor-Mediated Pathway. *PLoS ONE* 8, e71721.
279   doi:10.1371/journal.pone.0071721.

280 Buffo, A., Rite, I., Tripathi, P., Lepier, A., Colak, D., Horn, A.-P., Mori, T., and Götz, M. (2008).
281   Origin and progeny of reactive gliosis: A source of multipotent cells in the injured brain.
282   *Proc. Natl. Acad. Sci.* 105, 3581–3586. doi:10.1073/pnas.0709002105.

283 Chander, B. S., and Chakravarthy, V. S. (2012). A Computational Model of Neuro-Glio-Vascular
284   Loop Interactions. *PLoS One* 7, e48802. doi:10.1371/journal.pone.0048802.

285 David, O., and Friston, K. J. (2003). A neural mass model for MEG/EEG: coupling and neuronal
286   dynamics. *NeuroImage* 20, 1743–1755.

287 DiNuzzo, M., Gili, T., Maraviglia, B., and Giove, F. (2011). Modeling the contribution of neuron-
288   astrocyte cross talk to slow blood oxygenation level-dependent signal oscillations. *J.
289   Neurophysiol.* 106, 3010–3018. doi:10.1152/jn.00416.2011.

290 Dmochowski, J. P., Datta, A., Bikson, M., Su, Y., and Parra, L. C. (2011). Optimized multi-electrode
291   stimulation increases focality and intensity at target. *J. Neural Eng.* 8, 046011.
292   doi:10.1088/1741-2560/8/4/046011.

293 Dutta, A. (2014). EEG-NIRS based low-cost screening and monitoring of cerebral microvessels
294   functionality. *International Stroke Conference 2014, At San Diego, Volume: Junior
295   Investigator Session II: Invited Symposium.*

296 Dutta, A., Chowdhury, S. R., Dutta, A., Sylaja, P. N., Guiraud, D., and Nitsche, M. . (2013). A
297   phenomological model for capturing cerebrovascular reactivity to anodal transcranial direct
298   current stimulation. in *2013 6th International IEEE/EMBS Conference on Neural Engineering
299   (NER)*, 827–830. doi:10.1109/NER.2013.6696062.

Dutta, A., Jacob, A., Chowdhury, S. R., Das, A., and Nitsche, M. A. (2015). EEG-NIRS Based Assessment of Neurovascular Coupling During Anodal Transcranial Direct Current Stimulation - a Stroke Case Series. *J. Med. Syst.* 39, 205. doi:10.1007/s10916-015-0205-7.

Dutta, A., and Nitsche, M. . (2013). Neural mass model analysis of online modulation of electroencephalogram with transcranial direct current stimulation. in *2013 6th International IEEE/EMBS Conference on Neural Engineering (NER)*, 206–210. doi:10.1109/NER.2013.6695908.

Fricke, K., Seeber, A. A., Thirugnanasambandam, N., Paulus, W., Nitsche, M. A., and Rothwell, J. C. (2011). Time course of the induction of homeostatic plasticity generated by repeated transcranial direct current stimulation of the human motor cortex. *J. Neurophysiol.* 105, 1141–1149. doi:10.1152/jn.00608.2009.

Friston, K. J., Mechelli, A., Turner, R., and Price, C. J. (2000). Nonlinear responses in fMRI: the Balloon model, Volterra kernels, and other hemodynamics. *NeuroImage* 12, 466–477. doi:10.1006/nimg.2000.0630.

Girouard, H., and Iadecola, C. (2006). Neurovascular coupling in the normal brain and in hypertension, stroke, and Alzheimer disease. *J. Appl. Physiol. Bethesda Md 1985* 100, 328–335. doi:10.1152/japplphysiol.00966.2005.

Gonzalez-Lima, F., and Barrett, D. W. (2014). Augmentation of cognitive brain functions with transcranial lasers. *Front. Syst. Neurosci.* 8. doi:10.3389/fnsys.2014.00036.

Gruetter, R., Novotny, E. J., Boulware, S. D., Rothman, D. L., and Shulman, R. G. (1996). 1H NMR Studies of Glucose Transport in the Human Brain. *J. Cereb. Blood Flow Metab.* 16, 427–438. doi:10.1097/00004647-199605000-00009.

Halnes, G., ?stby, I., Pettersen, K. H., Omholt, S. W., and Einevoll, G. T. (2013). Electrodiffusive Model for Astrocytic and Neuronal Ion Concentration Dynamics. *PLoS Comput. Biol.* 9. doi:10.1371/journal.pcbi.1003386.

Han, C.-H., Song, H., Kang, Y.-G., Kim, B.-M., and Im, C.-H. (2014). Hemodynamic responses in rat brain during transcranial direct current stimulation: a functional near-infrared spectroscopy study. *Biomed. Opt. Express* 5, 1812–1821. doi:10.1364/BOE.5.001812.

Horvath, J. C., Carter, O., and Forte, J. D. (2014). Transcranial direct current stimulation: five important issues we aren't discussing (but probably should be). *Front. Syst. Neurosci.* 8. doi:10.3389/fnsys.2014.00002.

Huang, N. E., Shen, Z., Long, S. R., Wu, M. C., Shih, H. H., Zheng, Q., Yen, N.-C., Tung, C. C., and Liu, H. H. (1998). The empirical mode decomposition and the Hilbert spectrum for nonlinear and non-stationary time series analysis. *Proc. R. Soc. Lond. Ser. Math. Phys. Eng. Sci.* 454, 903–995. doi:10.1098/rspa.1998.0193.

Iadecola, C. (2004). Neurovascular regulation in the normal brain and in Alzheimer's disease. *Nat. Rev. Neurosci.* 5, 347–360. doi:10.1038/nrn1387.

337 Islam, N., Aftabuddin, M., Moriwaki, A., Hattori, Y., and Hori, Y. (1995). Increase in the calcium
338   level following anodal polarization in the rat brain. *Brain Res.* 684, 206–208.

339 Jindal, U., Sood, M., Chowdhury, S. R., Das, A., Kondziella, D., and Dutta, A. (2015a). Corticospinal
340   excitability changes to anodal tDCS elucidated with NIRS-EEG joint-imaging: an ischemic
341   stroke study. in *ResearchGate* Available at:
342   http://www.researchgate.net/publication/277800701_Corticospinal_excitability_changes_to_a
343   nodal_tDCS_elucidated_with_NIRS-EEG_joint-imaging_an_ischemic_stroke_study
344   [Accessed July 8, 2015].

345 Jindal, U., Sood, M., Dutta, A., and Chowdhury, S. R. (2015b). Development of Point of Care Testing
346   Device for Neurovascular Coupling From Simultaneous Recording of EEG and NIRS During
347   Anodal Transcranial Direct Current Stimulation. *IEEE J. Transl. Eng. Health Med.* 3, 1–12.
348   doi:10.1109/JTEHM.2015.2389230.

349 Jolivet, R., Coggan, J. S., Allaman, I., and Magistretti, P. J. (2015). Multi-timescale Modeling of
350   Activity-Dependent Metabolic Coupling in the Neuron-Glia-Vasculature Ensemble. *PLoS
351   Comput Biol* 11, e1004036. doi:10.1371/journal.pcbi.1004036.

352 Jung, T.-P., Makeig, S., McKeown, M. J., Bell, A. J., Lee, T.-W., and Sejnowski, T. J. (2001).
353   Imaging brain dynamics using independent component analysis. *Proc. IEEE* 89, 1107–1122.
354   doi:10.1109/5.939827.

355 Khadka, N., Truong, D. Q., and Bikson, M. (2015). Principles of Within Electrode Current Steering1.
356   *J. Med. Devices* 9, 020947–020947. doi:10.1115/1.4030126.

357 Krause, B., Márquez-Ruiz, J., and Cohen Kadosh, R. (2013). The effect of transcranial direct current
358   stimulation: a role for cortical excitation/inhibition balance? *Front. Hum. Neurosci.* 7, 602.
359   doi:10.3389/fnhum.2013.00602.

360 Leontiev, O., and Buxton, R. B. (2007). Reproducibility of BOLD, perfusion, and CMRO2
361   measurements with calibrated-BOLD fMRI. *NeuroImage* 35, 175–184.
362   doi:10.1016/j.neuroimage.2006.10.044.

363 Lucas, S. J. E., Tzeng, Y. C., Galvin, S. D., Thomas, K. N., Ogoh, S., and Ainslie, P. N. (2010).
364   Influence of Changes in Blood Pressure on Cerebral Perfusion and Oxygenation.
365   *Hypertension* 55, 698–705. doi:10.1161/HYPERTENSIONAHA.109.146290.

366 Mangia, A. L., Pirini, M., and Cappello, A. (2014). Transcranial direct current stimulation and power
367   spectral parameters: a tDCS/EEG co-registration study. *Front. Hum. Neurosci.* 8.
368   doi:10.3389/fnhum.2014.00601.

369 Markus, H., and Cullinane, M. (2001). Severely impaired cerebrovascular reactivity predicts stroke
370   and TIA risk in patients with carotid artery stenosis and occlusion. *Brain* 124, 457–467.
371   doi:10.1093/brain/124.3.457.

372 Matsumoto, J., Fujiwara, T., Takahashi, O., Liu, M., Kimura, A., and Ushiba, J. (2010). Modulation
373   of mu rhythm desynchronization during motor imagery by transcranial direct current
374   stimulation. *J. Neuroengineering Rehabil.* 7, 27. doi:10.1186/1743-0003-7-27.

375 McKendrick, R., Parasuraman, R., and Ayaz, H. (2015). Wearable functional near infrared
376   spectroscopy (fNIRS) and transcranial direct current stimulation (tDCS): expanding vistas for
377   neurocognitive augmentation. *Front. Syst. Neurosci.*, 27. doi:10.3389/fnsys.2015.00027.

378 Meinzer, M., Lindenberg, R., Darkow, R., Ulm, L., Copland, D., and Flöel, A. (2014). Transcranial
379   direct current stimulation and simultaneous functional magnetic resonance imaging. *J. Vis.*
380   *Exp. JoVE*. doi:10.3791/51730.

381 Molaee-Ardekani, B., Márquez-Ruiz, J., Merlet, I., Leal-Campanario, R., Gruart, A., Sánchez-
382   Campusano, R., Birot, G., Ruffini, G., Delgado-García, J.-M., and Wendling, F. (2013).
383   Effects of transcranial Direct Current Stimulation (tDCS) on cortical activity:
384   A computational modeling study. *Brain Stimulat.* 6, 25–39. doi:10.1016/j.brs.2011.12.006.

385 Moore, C. I., and Cao, R. (2008). The hemo-neural hypothesis: on the role of blood flow in
386   information processing. *J. Neurophysiol.* 99, 2035–2047. doi:10.1152/jn.01366.2006.

387 Moran, R. J., Kiebel, S. J., Stephan, K. E., Reilly, R. B., Daunizeau, J., and Friston, K. J. (2007). A
388   neural mass model of spectral responses in electrophysiology. *NeuroImage* 37, 706–720.
389   doi:10.1016/j.neuroimage.2007.05.032.

390 Nikulin, V. V., Fedele, T., Mehnert, J., Lipp, A., Noack, C., Steinbrink, J., and Curio, G. (2014).
391   Monochromatic Ultra-Slow (~0.1Hz) Oscillations in the human electroencephalogram and
392   their relation to hemodynamics. *NeuroImage*. doi:10.1016/j.neuroimage.2014.04.008.

393 Nitsche, M. A., Fricke, K., Henschke, U., Schlitterlau, A., Liebetanz, D., Lang, N., Henning, S.,
394   Tergau, F., and Paulus, W. (2003). Pharmacological modulation of cortical excitability shifts
395   induced by transcranial direct current stimulation in humans. *J. Physiol.* 553, 293–301.
396   doi:10.1113/jphysiol.2003.049916.

397 Nitsche, M. A., and Paulus, W. (2000). Excitability changes induced in the human motor cortex by
398   weak transcranial direct current stimulation. *J. Physiol.* 527 Pt 3, 633–639.

399 Nitsche, M. A., and Paulus, W. (2011). Transcranial direct current stimulation--update 2011. *Restor.*
400   *Neurol. Neurosci.* 29, 463–492. doi:10.3233/RNN-2011-0618.

401 Notturno, F., Marzetti, L., Pizzella, V., Uncini, A., and Zappasodi, F. (2014). Local and remote effects
402   of transcranial direct current stimulation on the electrical activity of the motor cortical
403   network. *Hum. Brain Mapp.* 35, 2220–2232. doi:10.1002/hbm.22322.

404 Novak, V. (2012). Cognition and Hemodynamics. *Curr. Cardiovasc. Risk Rep.* 6, 380–396.
405   doi:10.1007/s12170-012-0260-2.

406 Nunez, P. L., and Srinivasan, R. (2006). *Electric Fields of the Brain: The Neurophysics of EEG*.
407   Oxford University Press.

408 Pellerin, L., and Magistretti, P. J. (1994). Glutamate uptake into astrocytes stimulates aerobic
409   glycolysis: a mechanism coupling neuronal activity to glucose utilization. *Proc. Natl. Acad.*
410   *Sci. U. S. A.* 91, 10625–10629.

411 Polanía, R., Nitsche, M. A., and Paulus, W. (2011). Modulating functional connectivity patterns and
412   topological functional organization of the human brain with transcranial direct current
413   stimulation. *Hum. Brain Mapp.* 32, 1236–1249. doi:10.1002/hbm.21104.

414 Polanía, R., Paulus, W., and Nitsche, M. A. (2012). Modulating cortico-striatal and thalamo-cortical
415   functional connectivity with transcranial direct current stimulation. *Hum. Brain Mapp.* 33,
416   2499–2508. doi:10.1002/hbm.21380.

417 Pulgar, V. M. (2015). Direct electric stimulation to increase cerebrovascular function. *Front. Syst.*
418   *Neurosci.* 9, 54. doi:10.3389/fnsys.2015.00054.

419 Raffin, E., and Siebner, H. R. (2014). Transcranial brain stimulation to promote functional recovery
420   after stroke. *Curr. Opin. Neurol.* 27, 54–60. doi:10.1097/WCO.0000000000000059.

421 Rahman, A., Reato, D., Arlotti, M., Gasca, F., Datta, A., Parra, L. C., and Bikson, M. (2013). Cellular
422   effects of acute direct current stimulation: somatic and synaptic terminal effects. *J. Physiol.*
423   591, 2563–2578. doi:10.1113/jphysiol.2012.247171.

424 Schestatsky, P., Morales-Quezada, L., and Fregni, F. (2013). Simultaneous EEG Monitoring During
425   Transcranial Direct Current Stimulation. *J. Vis. Exp. JoVE*. doi:10.3791/50426.

426 Schiff, S. J., and Sauer, T. (2008). Kalman filter control of a model of spatiotemporal cortical
427   dynamics. *J. Neural Eng.* 5, 1–8. doi:10.1088/1741-2560/5/1/001.

428 Siesler, H. W., Ozaki, Y., Kawata, S., and Heise, H. M. (2008). *Near-Infrared Spectroscopy:*
429   *Principles, Instruments, Applications*. John Wiley & Sons.

430 Sigala, R., Haufe, S., Roy, D., Dinse, H. R., and Ritter, P. (2014). The role of alpha-rhythm states in
431   perceptual learning: insights from experiments and computational models. *Front. Comput.*
432   *Neurosci.* 8, 36. doi:10.3389/fncom.2014.00036.

433 Sood, M., Jindal, U., Chowdhury, S. R., Das, A., Kondziella, D., and Dutta, A. (2015). Anterior
434   temporal artery tap to identify systemic interference using short-separation NIRS
435   measurements: a NIRS/EEG-tDCS study. in *ResearchGate* Available at:
436   http://www.researchgate.net/publication/277710873_Anterior_temporal_artery_tap_to_identif
437   y_systemic_interference_using_short-separation_NIRS_measurements_a_NIRSEEG-
438   tDCS_study [Accessed July 8, 2015].

439 Sotero, R. C., Trujillo-Barreto, N. J., Iturria-Medina, Y., Carbonell, F., and Jimenez, J. C. (2007).
440   Realistically coupled neural mass models can generate EEG rhythms. *Neural Comput.* 19,
441   478–512. doi:10.1162/neco.2007.19.2.478.

442 Spitoni, G. F., Cimmino, R. L., Bozzacchi, C., Pizzamiglio, L., and Di Russo, F. (2013). Modulation
443   of spontaneous alpha brain rhythms using low-intensity transcranial direct-current
444   stimulation. *Front. Hum. Neurosci.* 7, 529. doi:10.3389/fnhum.2013.00529.

445 Suzuki, A., Stern, S. A., Bozdagi, O., Huntley, G. W., Walker, R. H., Magistretti, P. J., and Alberini, C.
446   M. (2011). Astrocyte-neuron lactate transport is required for long-term memory formation.
447   *Cell* 144, 810–823. doi:10.1016/j.cell.2011.02.018.

448   Ursino, M., Cona, F., and Zavaglia, M. (2010). The generation of rhythms within a cortical region:
449   analysis of a neural mass model. *NeuroImage* 52, 1080–1094.
450   doi:10.1016/j.neuroimage.2009.12.084.

451   Volterra, A., Liaudet, N., and Savtchouk, I. (2014). Astrocyte Ca^{2+} signalling: an unexpected
452   complexity. *Nat. Rev. Neurosci.* 15, 327–335. doi:10.1038/nrn3725.

453   Whalen, A. J., Brennan, S. N., Sauer, T. D., and Schiff, S. J. (2015). Observability and Controllability
454   of Nonlinear Networks: The Role of Symmetry. *Phys. Rev. X* 5, 011005.
455   doi:10.1103/PhysRevX.5.011005.

456   Yang, J., Ruchti, E., Petit, J.-M., Jourdain, P., Grenningloh, G., Allaman, I., and Magistretti, P. J.
457   (2014). Lactate promotes plasticity gene expression by potentiating NMDA signaling in
458   neurons. *Proc. Natl. Acad. Sci.* 111, 12228–12233. doi:10.1073/pnas.1322912111.

459   Zaehle, T., Sandmann, P., Thorne, J. D., Jäncke, L., and Herrmann, C. S. (2011). Transcranial direct
460   current stimulation of the prefrontal cortex modulates working memory performance:
461   combined behavioural and electrophysiological evidence. *BMC Neurosci.* 12, 2.
462   doi:10.1186/1471-2202-12-2.

463   Zavaglia, M., Astolfi, L., Babiloni, F., and Ursino, M. (2006). A neural mass model for the simulation
464   of cortical activity estimated from high resolution EEG during cognitive or motor tasks. *J.*
465   *Neurosci. Methods* 157, 317–329. doi:10.1016/j.jneumeth.2006.04.022.

466   Zheng, X., Alsop, D. C., and Schlaug, G. (2011). Effects of transcranial direct current stimulation
467   (tDCS) on human regional cerebral blood flow. *NeuroImage* 58, 26–33.
468   doi:10.1016/j.neuroimage.2011.06.018.

469

470 **Figure legends**

471 **Figure 1:** Illustration of the effects of transcranial direct current stimulation (tDCS) from
472 simultaneous recording of electroencephalogram (EEG) and near infra red spectroscopy (NIRS). The
473 colors on the plot corresponds to the sensors. Here, only one anode and one cathode is highlighted for
474 tDCS, however, local current steering based on NIRS-EEG feedback is possible to optimally orient
475 the electric field with multiple return electrodes (Khadka et al., 2015). NVU consists of the
476 endothelium, glia, neurons, pericytes, and the basal lamina in which neurons, astrocytes, and vessels
477 are semi-independent networks operating in tandem. Neuronal network activity drives functional
478 hyperemia via direct effects on the blood vessels network as well as indirect effects via the astrocytic
479 network. Also, the hemodynamics changes can impact neuronal network activity via direct (diffusible
480 messengers, electromechanical and thermal interactions) and indirect (via astrocytic network)
481 pathways.
482
483 **Figure 2:** State modulation of the neurovascular unit (NVU) with transcranial direct current
484 stimulation (tDCS) to facilitate a brain state, e.g., spatiotemporal alpha-rhythm state. F is the function
485 to capture NVU system, W is the function to capture observations, ICA is independent component
486 (IC) analysis is a linear decomposition method to transform electroencephalogram (EEG) - near
487 infrared spectroscopy (NIRS) data collected at single scalp channels to a spatially transformed
488 "virtual channel" (i.e., a spatial filter on multi-channel EEG-NIRS data), EMD is empirical model
489 decomposition of the "virtual channel" observations that provide intrinsic mode functions (IMF) for
490 proportional control (gain is G) of individual "virtual channel" activity or IC (e.g., posterior alpha
491 band activity) with tDCS.